J. Fluid Mech. (1975), *vol.* 69, *part* 2, *pp.* 353–375
Printed in Great Britain

Experimental results for the transpired turbulent boundary layer in an adverse pressure gradient

By P. S. ANDERSEN,
Danish Atomic Energy Commission, Research Establishment Risø, Roskilde

W. M. KAYS AND R. J. MOFFAT
Department of Mechanical Engineering, Stanford University,
Stanford, California 94305

(Received 5 September 1973)

An experimental investigation of the fluid mechanics of the transpired turbulent boundary layer in zero and adverse pressure gradients was carried out on the Stanford Heat and Mass Transfer Apparatus. Profiles of (*a*) the mean velocity, (*b*) the intensities of the three components of the turbulent velocity fluctuations and (*c*) the Reynolds stress were obtained by hot-wire anemometry. The wall shear stress was measured by using an integrated form of the boundary-layer equation to 'extrapolate' the measured shear-stress profiles to the wall.

The two experimental adverse pressure gradients corresponded to free-stream velocity distributions of the type $u_\infty \propto x^m$, where $m = -0{\cdot}15$ and $-0{\cdot}20$, x being the streamwise co-ordinate. Equilibrium boundary layers (i.e. flows with velocity defect profile similarity) were obtained when the transpiration velocity v_0 was varied such that the blowing parameter $B \equiv \rho v_0 u_\infty/\tau_0$ and the Clauser pressure-gradient parameter $\beta \equiv \delta_1 \tau_0^{-1}\, dp/dx$ were held constant. (τ_0 is the shear stress at the wall and δ_1 is the displacement thickness.)

Tabular and graphical results are presented.

1. Introduction

The Heat and Mass Transfer Group at Stanford University has since 1967 been engaged in a continuous effort directed towards understanding transpired turbulent boundary layers. The fluid mechanics of constant-pressure boundary layers (Simpson, Moffat & Kays 1969) and boundary layers in favourable pressure gradients (Julien, Kays & Moffat 1971; Loyd, Moffat & Kays 1970) have so far been studied experimentally. Kays (1972) summarizes the findings for these flows.

Only one experimental study of turbulent boundary layers in adverse pressure gradients with transpiration has been reported in the literature. McLean & Mellor (1972) have studied blown turbulent boundary layers in very strong adverse pressure gradients. The main objective of their work was to study the onset of separation. McLean & Mellor did not, however, *measure* the skin friction, but instead relied on Stevenson's (1963) law of the wall.

In the present work the wall shear stress was determined by measuring the shear stress away from the wall (as the sum of the Reynolds stress and the viscous stress) and extrapolating to the wall by integrating the boundary-layer equations for the shear-stress profile. This technique should give a degree of 'independence' to the present data.

In addition to investigating adverse-pressure-gradient boundary layers, which are the main focus of the present work, it seemed natural to repeat some of the constant-pressure flows of Simpson *et al.* using the new technique for the measurement of skin friction. A secondary motivation for doing this was the finding, during exploratory tests, that the mean velocity profiles obtained by hot-wire anemometry differed appreciably (especially very close to the wall) from the earlier results obtained by Simpson *et al.* using a flattened Pitot tube.

An attempt was made to remove all complicating circumstances from the basic problem of obtaining accurate measurements of transpired turbulent boundary layers. The investigation was therefore limited to low-speed constant-property flows with the transpiration fluid being the same as the free-stream fluid (air). Boundary conditions leading to strong deviations from 'equilibrium' (e.g. steps in the pressure gradient or in the transpiration rate) were avoided. Adverse pressure gradients strong enough to cause separation were also outside the scope of this investigation.

The concept of the equilibrium boundary layer introduced by Clauser (1954) was extended to include a class of boundary layers with transpiration. The 'outer-region similarity' defining an equilibrium boundary layer implies that the 'defect profile' is invariant with x. The Clauser shape factor

$$G = \int_0^\infty \left(\frac{u_\infty - u}{u_\tau}\right)^2 dy \Big/ \int_0^\infty \frac{u_\infty - u}{u_\tau} dy, \tag{1}$$

where u is the mean streamwise velocity and u_τ is the friction velocity, is therefore a constant for an equilibrium boundary layer. (This is only approximately true since the 'wall region' does contribute slightly to the integrals in the definition (1) of G and is not self-similar in these co-ordinates.)

The momentum integral equation for a transpired boundary layer may be written in the form

$$d(\delta_2 u_\infty^2)/dx = (\tau_0/\rho)(1+\beta+B), \tag{2}$$

where

$$\delta_2 \equiv \int_0^\infty \frac{u}{u_\infty}\left(1-\frac{u}{u_\infty}\right) dy$$

is the momentum thickness. The Clauser pressure-gradient parameter

$$\beta \equiv (\delta_1/\tau_0)\, dp/dx,$$

where

$$\delta_1 \equiv \int_0^\infty \left(1-\frac{u}{u_\infty}\right) dy$$

is the displacement thickness, may be interpreted as the ratio between the contributions of the pressure and the shear stress to the production of momentum defect in the boundary layer. $B \equiv \rho v_0 u_\infty/\tau_0$ will be called the 'blowing parameter'; it is the ratio between the contributions of the transpiration fluid and

the wall shear stress to the production of momentum defect in the boundary layer. Clauser has found experimentally that non-transpired ($B = 0$) equilibrium boundary layers are obtained when the acceleration parameter β is held constant. For flows with zero pressure gradient the results of Simpson *et al.* (1969) indicate that boundary layers with $\beta = 0$ and $B =$ constant are also equilibrium boundary layers. It was therefore reasonable to hope that keeping β *and* B constant (but different from zero) would result in equilibrium boundary layers in adverse pressure gradients with transpiration.

The complete set of hydrodynamic data obtained on adverse-pressure-gradient flows with transpiration may be found in Andersen, Kays & Moffat (1972). That reference also contains a fuller account of the motivation and background for the present work.

2. Experimental boundary conditions

A few reasonable assumptions permit prediction of the boundary conditions ($u_\infty = u_\infty(x)$ and $v_0/u = F(x)$) which will produce a constant acceleration parameter β and blowing parameter B simultaneously. The assumptions are as follows.

$$(a) \quad u_\infty \propto x^m, \quad \text{where} \quad m \leqslant 0.$$

This free-stream velocity variation is known to lead to equilibrium boundary layers in the non-transpired ($B = 0$) case (Bradshaw 1967).

$$(b) \quad (c_f/c_{f0})_{m,\,Re} = f(B),$$

where Re is the momentum-thickness Reynolds number and $\frac{1}{2}c_f \equiv \tau_0/\rho u^2$ is the friction coefficient, $\frac{1}{2}c_{f0}$ being its value for $v_0 = 0$. This equation expresses the assumption that the ratio of the friction coefficient for the transpired boundary layer to that for the corresponding (same m) non-transpired boundary layer at the same momentum-thickness Reynolds number is a unique function of the blowing parameter B. This assumption has been verified by Simpson *et al.* (1969) for the case of constant-pressure ($m = 0$) boundary layers.

$$(c) \quad \tfrac{1}{2}c_{f0} = a\,Re^{-b}.$$

This friction law for the non-transpired boundary layer is, of course, always valid for a small enough range of the Reynolds number Re.

Assumptions (a), (b) and (c) combined with the momentum equation (2) lead to the result that the desired transpiration boundary condition should be

$$F(x) \propto x^{m_F}, \quad \text{where} \quad m_F = -b(1+m)/(1+b).$$

This variation of the blowing fraction, together with the free-stream velocity variation $u_\infty \propto x^m$, was shown experimentally to lead to boundary layers having both a constant acceleration parameter β and blowing parameter B. Boundary layers with $F =$ constant were also established experimentally.

3. Experimental apparatus, instrumentation and procedure

The work was carried out on the Stanford Heat and Mass Transfer Apparatus, an open-ended wind tunnel with a porous floor in the test section and a secondary air system for supply and metering of the transpiration air. The basic wind tunnel has been very adequately described by previous experimenters (for example Moffat & Kays 1968); we shall therefore concentrate the description here on modifications introduced to permit the present work on adverse pressure gradients.

The test section is an 8 ft long straight duct with a rectangular cross-section (20 in. wide and 6 in. high). The test plate (the floor of the test section) is composed of 24 porous plates each 18 in. wide and 4 in. in the direction of the main flow. The transpiration air system permits control and measurement of the flow rate for each individual plate. The porous plates are 0·25 in. thick and made of sintered bronze material composed of particles with diameters between 0·0023 and 0·007 in. The porosity is approximately 40 % and the flow-rate uniformity is within $\pm 6\,\%$ in the centre 6 in. span. The flow resistance offered by the plates is large enough for the uniformity of the transpiration velocity not to be significantly affected by the pressure gradients in the main flow.

One of the side walls contains square-edged holes 0·040 in. in diameter for static-pressure taps drilled with a 2 in. pitch 1 in. above the test plate. These static-pressure taps were used in connexion with a Kiel probe in the free stream for the measurement of the free-stream dynamic-pressure distribution.

The top plate has 23 transverse slots located at 4 in. intervals in the streamwise direction. Since the tunnel is operated with a static pressure in the test section slightly above ambient, the streamwise velocity distribution in the tunnel may be controlled by adjusting the individual slot widths.

The length of the slots (in the lateral direction) may be restricted by movable 'fingers'. These permit the length of the slots to be equal to or less than the width of the tunnel. This feature was incorporated because Clauser (1954) had reported a lateral divergence of the streamlines in the bottom-wall boundary layer of a wind tunnel where an adverse pressure gradient was generated by removal of air through slots in the top wall. Tests were carried out in the present tunnel both with the fingers flush with the side walls and with the slot lengths restricted by up to 0·5 in. on each side. No significant effect on the rate of growth $d\delta_2/dx$ of the test-plate boundary layer was found.

Each of the 24 plates that form the top wall has an access hole at the centre-line of the test section. Every third plate has 8 additional access holes at 2 in. intervals in the transverse direction. When not in use the access holes are closed with plugs which are flush with the inside of the top plates.

The free-stream velocity distribution was computed from the dynamic-pressure distribution using Bernoulli's equation. However, all velocity profiles and turbulence profiles were obtained by linearized constant-temperature hot-wire anemometry. One reason why Pitot tubes (which are more convenient to use) were discarded was that serious discrepancies were found in turbulent shear flow between measurements by tubes with rounded and flattened mouths. As an example figure 1 shows experimental mean velocity profiles obtained with

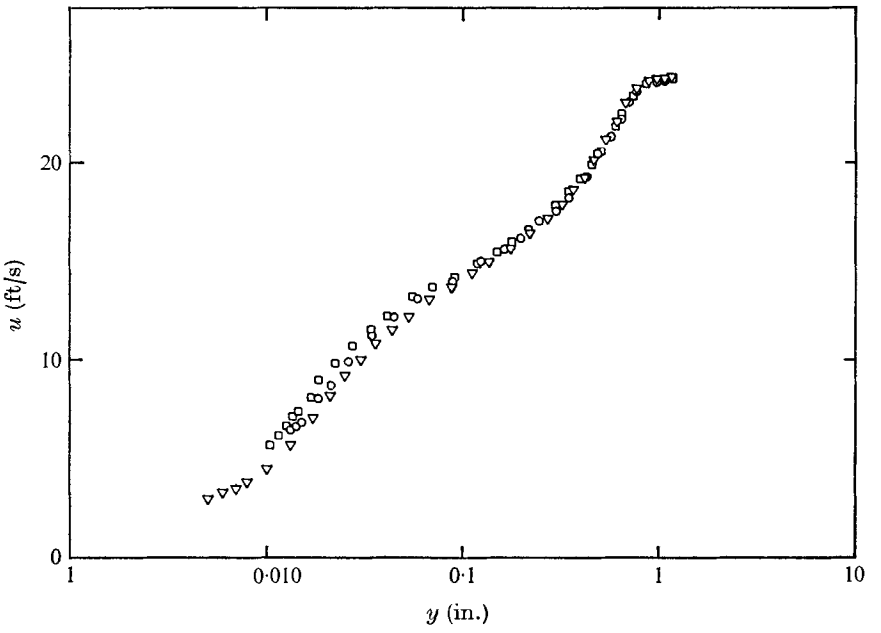

FIGURE 1. Comparison of probes. Velocity profile in a 'weak' adverse pressure gradient ($m = -0{\cdot}15$). No transpiration. □, Pitot tube, flattened mouth (external height = 0·015 in., width = 0·032 in., wall thickness = 0·002 in.); ○, Pitot tube, round mouth (external diameter = 0·02 in., wall thickness = 0·002 in.); ▽, hot wire.

a round-mouthed (0·020 in. O.D., wall thickness 0·002 in.) and a flattened-mouthed Pitot tube (external height = 0·015 in., width = 0·032 in., wall thickness 0·002 in.) in an adverse-pressure-gradient non-transpired boundary layer. The Young & Maas (1936) shear correction was applied for both Pitot probes. It is obvious from figure 1 that the two Pitot probes disagree greatly in the inner regions of the boundary layer. The disagreement would have been even greater without the shear correction. Also shown in the figure is the velocity profile obtained by hot-wire anemometry.

The mean velocities are 6 s averages. The mean-square value of the linearizer output was read by a Thermosystems r.m.s. voltmeter Model 1060 with the time constant set at 10 s. The mean-square output from the r.m.s. voltmeter was averaged over 200 s to reduce the random scatter to below 1 %.

A horizontal hot wire was used for the measurement of u and the r.m.s. streamwise velocity fluctuation $\overline{u'^2}$. The wire was platinum, 0·0002 in. diameter and 0·080 in. long. The overheat ratio was about 1·6.

A rotatable hot wire with gold-plated ends (DISA 55F02 hot-wire element) slanted at 45° was used for the measurement of $\overline{u'v'}$ and (in connexion with the horizontal wire) of $\overline{v'^2}$ and $\overline{w'^2}$. The probe spindle could be placed in six angular positions. Since only three are necessary for the measurement of $\overline{u'^2}$, $\overline{v'^2}$, $\overline{w'^2}$ and $\overline{u'v'}$ the redundancy could be used to reduce experimental scatter and errors due to possible slight lateral misalignments of the probe axis.

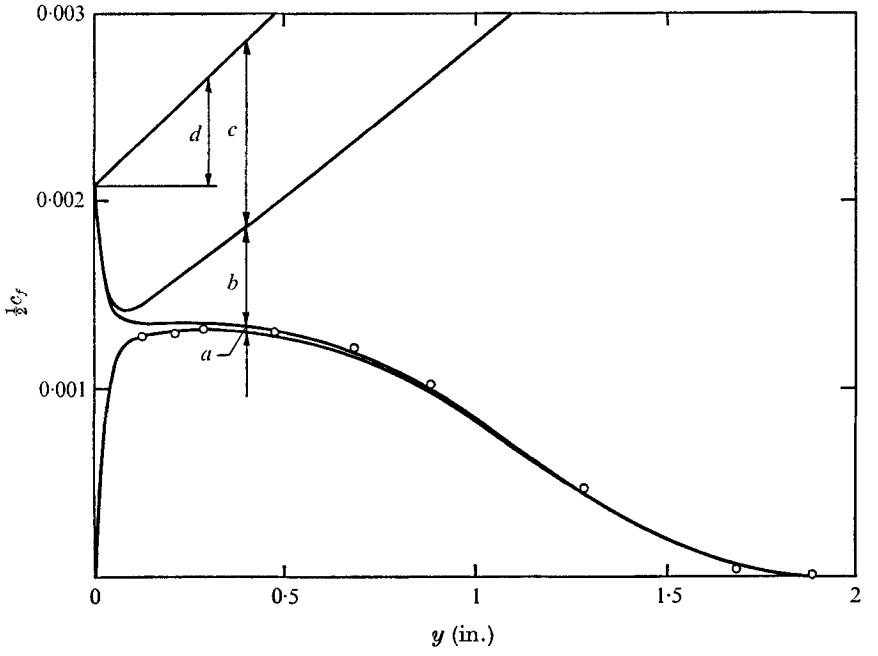

FIGURE 2. Graphical illustration of the method of evaluating the friction coefficient $\frac{1}{2}c_f$ from (3). Weak adverse pressure gradient with suction ($m = -0{\cdot}15$, $m_F = -0{\cdot}17$, $F_1 = -0{\cdot}002$). ○, measured values of the Reynolds stress $-\overline{u'v'}/u^2$; ——, profile of $-\overline{u'v'}/u_\infty^2$ computed from (3), $\frac{1}{2}c_f$ having been adjusted such that the computed profile passes through the measured Reynolds stress closest to the wall. The various terms in (3) are represented by

$a \equiv (\nu/u_\infty^2)\,\partial u/\partial y$, viscous shear stress,

$b \equiv \frac{1}{u_\infty^2}\left(u\int_0^y \frac{\partial u}{\partial x}dy - 2\int_0^y u\frac{\partial u}{\partial x}dy\right)$, convective contribution,

$c \equiv uv_0/u_\infty^2$, contribution due to transpiration,

$d \equiv (y/u_\infty)\,du_\infty/dx$, contribution due to the pressure gradient.

4. Measurement of wall shear stress

By integrating the time-averaged boundary-layer equations for incompressible flow one may obtain the following equation for the friction coefficient (the Reynolds-stress term $-\partial(\overline{u'^2})/\partial x$ has been neglected):

$$-\frac{\overline{u'v'}}{u_\infty^2} = \frac{c_f}{2} - \frac{y}{u_\infty}\frac{du_\infty}{dx} + \frac{uv_0}{u_\infty^2} - \frac{1}{u_\infty^2}\left(u\int_0^y \frac{\partial u}{\partial x}dy - 2\int_0^y u\frac{\partial u}{\partial x}dy\right) - \frac{\nu}{u_\infty^2}\frac{\partial u}{\partial y} + 3D(y),$$

where
$$3D(y) = \frac{1}{u_\infty^2}\left(\int_0^y u\frac{\partial w}{\partial z}dy - u\int_0^y \frac{\partial w}{\partial z}dy\right) \quad \text{for} \quad w = 0. \tag{3}$$

For small values of y (close to the wall) the term $3D(y)$, which accounts for the deviation from the ideal of two-dimensionality, must be truly vanishing. Therefore, by measuring the Reynolds stress $-\rho\overline{u'v'}$ close to the wall, the friction coefficient $\frac{1}{2}c_f$ may be computed from (3) if the mean flow field $u(x, y)$ and the

transpiration velocity v_0 have also been measured. This method of measuring the skin friction avoids the problems with 'three-dimensionality' encountered when one attempts to use the von Kármán momentum integral equation to obtain very small friction coefficients.

The integrals were evaluated by numerical integration of the measured mean velocity profiles, assuming a linear velocity profile inside the innermost point. The value of y^+ ($\equiv yu_\tau/\nu$) at this point was in all cases smaller than 6.

Figure 2 illustrates by an example the magnitude of the various terms in (3). The Reynolds stress measured closest to the wall (at $y \approx 0{\cdot}1$ in.) was used for the determination of the friction coefficient. Note in particular in figure 2 that the convective term, containing the integrals of the x derivatives of the velocity (and represented by b in figure 2), is insignificant close to the wall.

Once the friction coefficient $\frac{1}{2}c_f$ has been determined, the dimensionless Reynolds-stress profile may be computed from (3) using the value of $\frac{1}{2}c_f$ and the mean velocity profiles. Figure 2 indicates very close agreement between the computed and the measured Reynolds-stress profiles.

5. Experimental results

The boundary conditions realized experimentally may nominally be expressed by

$$u_\infty = u_1\left(\frac{x-x_0}{x_1-x_0}\right)^m, \quad F = F_1\left(\frac{x-x_0}{x_1-x_0}\right)^{m_F}, \tag{4), (5}$$

where the values of the constants u_1, F_1, x_0, x_1, m and m_F are summarized in table 1. The non-zero values of m_F satisfy the condition $m_F = -(1+m)b/(1+b)$, and correspond to boundary layers having $B =$ constant. The values of x_0 are chosen to correspond (approximately) to the virtual origin of the turbulent boundary layer. The virtual origin $x_{0,\,\mathrm{meas}}$ was determined by least-squares fitting the measured momentum thicknesses with an equation of the form $\delta_{2,\,\mathrm{fit}} = \alpha(x-x_{0,\,\mathrm{meas}})^\gamma$, where α and γ were 'free' during the minimization process.

All the measured friction coefficients are plotted in figures 3 (*a*)–(*d*) as functions of the momentum-thickness Reynolds number Re. The friction coefficients for the three non-transpired boundary layers were fitted by equations of the form

$$\tfrac{1}{2}c_{f0} = a\,Re^{-0{\cdot}25}. \tag{6}$$

The best fits were obtained for the values of the constant a given in table 2.

The friction coefficients for the transpired boundary layers may be fitted with expressions of the form

$$(c_f/c_{f0})_{m,\,Re} = f_0(B_0), \tag{7}$$

where

$$B_0 \equiv F/(\tfrac{1}{2}c_{f0}) \tag{8}$$

is a 'modified' blowing parameter. The relationship (7) is mathematically equivalent to the expression

$$(c_f/c_{f0})_{m,\,Re} = f(B), \tag{9}$$

which was shown by Simpson *et al.* (1969) to correlate their experimental results for constant-pressure ($m = 0$) boundary layers.

m	u_1 (ft/s)	x_0 (in.)	x_1 (in.)	F_1	m_F
0	31·1	—	—	0	—
				0·001	
				0·002	0
				0·00375	
				0·008	
−0·15	29·2	−3	4	0	—
				± 0·001	
				± 0·002	0 and −0·17
				± 0·004	
−0·20	29·2	−2	4	−0·002	−0·16
				0	—

TABLE 1. Experimental boundary conditions (nominal)

m	a	Experimental range for Re
0	0·0120	850–3100
−0·15	0·0102	1500–3500
−0·20	0·0083	1700–4100

TABLE 2. Coefficients for best fit (6) of the unblown friction coefficients

Figure 4 shows experimental values of $(c_f/c_{f0})_{m,Re}$ for all three experimental values of m plotted versus the modified blowing parameter B_0. It may be observed that the same function $f_0(B_0)$ might adequately correlate the results for all three pressure gradients. The correlation used by Simpson *et al.* for their constant-pressure boundary layers, i.e. $c_f/c_{f0} = [\ln(1+B)/B]^{0.7}$, with $B = B_0/(c_f/c_{f0})_{Re}$, is indicated in the figure for easy comparison.

Simpson *et al.* correlated their *unblown* friction coefficients using $a = 0{\cdot}0130$ in (6), i.e. a value 8 % higher than the one proposed here. This discrepancy together with the overprediction of the present transpired data by Simpson's correlation (as shown evidenced by figure 4) indicates that the present friction coefficients are lower than those measured by Simpson *et al.*

The Clauser shape factor G is plotted versus $\beta + B$ in figure 5. It may be observed that runs for which β and B are constant (filled symbols) correspond to equilibrium boundary layers in the sense that G is constant for these runs. The open symbols correspond to runs having F = constant. It may be noted that G is the same function of $\beta + B$ for all the experimental boundary layers; this means that the F = constant boundary layers are sufficiently close to equilibrium for only local values of β and B to matter for the shape of the defect velocity profile and furthermore for β and B to have identical effects upon the shape of the near-equilibrium velocity defect profile.

Examples of mean velocity profiles in wall co-ordinates are shown in figure 6 (*a*) for non-transpired boundary layers and in figure 6 (*b*) for the $m = -0{\cdot}15$ family

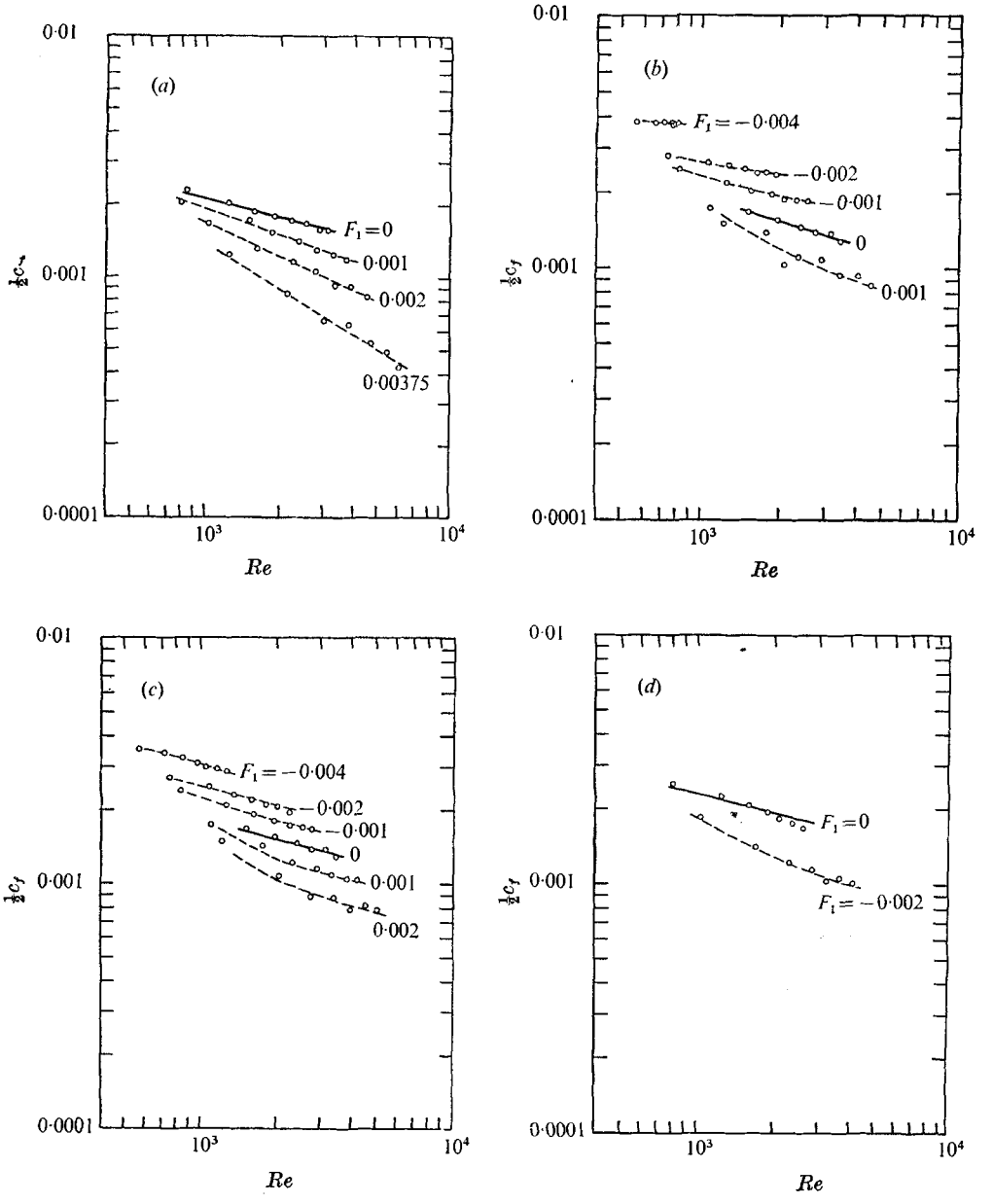

FIGURE 3. Friction coefficients *vs.* momentum-thickness Reynolds number. (*a*) Constant pressure ($m = 0$) with constant blowing fractions. (*b*) 'Weak' adverse pressure gradient ($m = -0·15$) with constant blowing fractions. (*c*) 'Weak' adverse pressure gradient ($m = -0·15$); transpiration boundary condition according to (5) (equilibrium boundary layers). (*d*) 'Strong' adverse pressure gradient ($m = -0·20$); transpiration boundary condition according to (5) (equilibrium boundary layers). ○, measured values; – – –, visual aid only; ——, fit of unblown data by (6).

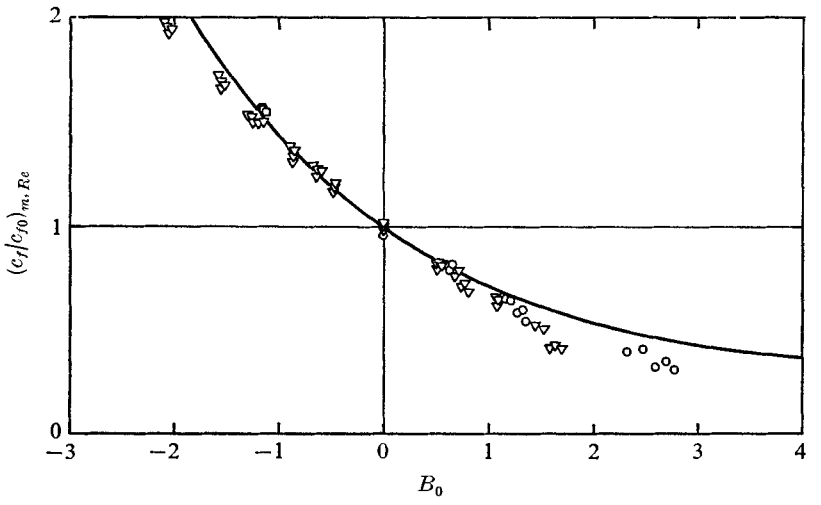

FIGURE 4. Friction coefficient ratios *vs.* modified blowing parameter $B_0 = F/(\frac{1}{2}c_{f0})$. Data for $35 \leqslant x \leqslant 82$ in. ○, $m = 0$; ▽, $m = -0{\cdot}15$; □, $m = -0{\cdot}20$; —, $(c_f/c_{f0})_{Re} = [\ln(1+B)/B]^{0{\cdot}7}$, $B = B_0/(c_f/c_{f0})_{Re}$ (Simpson *et al.* 1969).

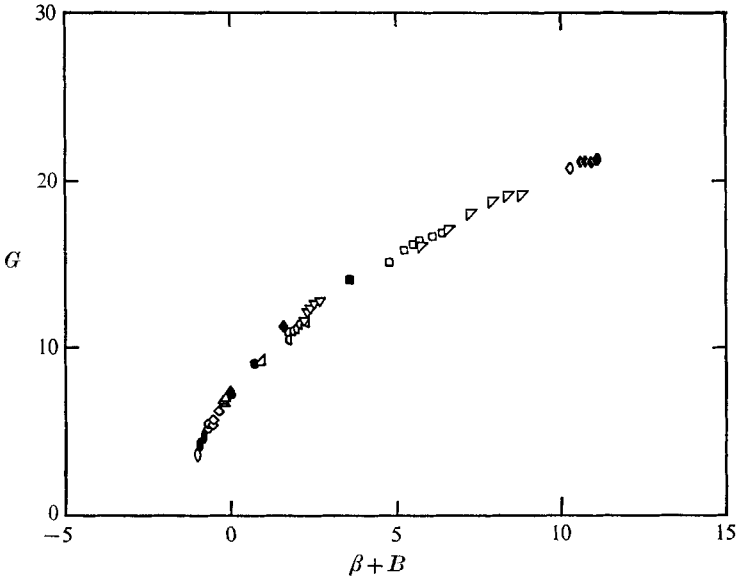

FIGURE 5. Clauser shape factor *vs.* sum of the Clauser pressure-gradient parameter and the blowing parameter.

	⬮	◿	◻	▽	○	⬮	◇	◆	△
m	0	0	0	0	−1·15	−1·15	−1·15	−1·15	−1·15
F_1	0	−0·001	−0·002	−0·00375	−0·004	−0·004	−0·002	−0·002	−0·001
m_F	0	0	0	0	0	−0·17	0	−0·17	0

	▲	●	▽	▼	■	◻	◀	◆	⬮
m	−1·15	−1·15	−1·15	−1·15	−1·15	−1·15	−1·15	−0·20	−0·20
F_1	−0·001	0	0·001	0·001	0·002	0·002	0·004	0	−0·002
m_F	−0·17	0	−0·17	0	−0·17	0	−0·17	0	−0·16

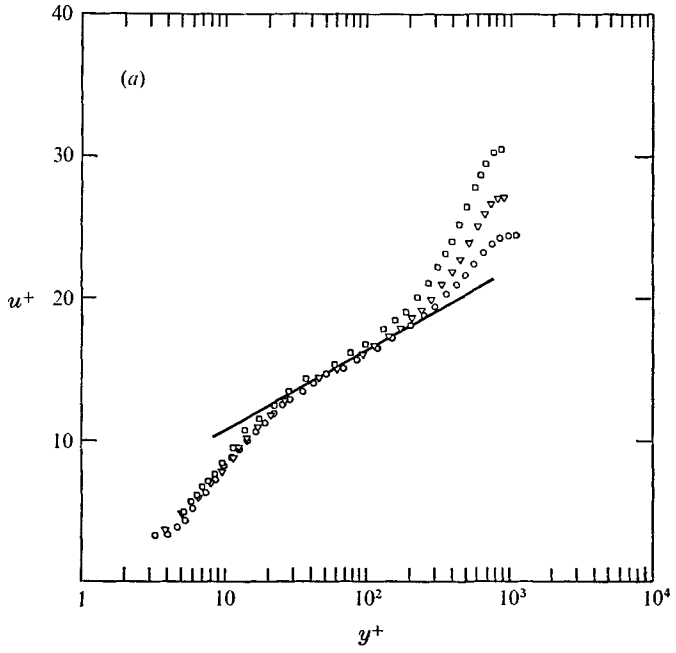

FIGURE 6(*a*). For legend see next page.

of transpired equilibrium boundary layers. It may be readily observed that the classical law of the wall

$$u^+ = \frac{1}{0{\cdot}41} \ln y^+ + 5{\cdot}0 \tag{10}$$

(constants from Coles 1962) fits the 'logarithmic region' of the non-transpired profiles, whereas the transpired profiles may deviate considerably.

The mixing length l, defined by

$$-\overline{u'v'} = l^2(du/dy)^2, \tag{11}$$

is presented in figure 7 (*a*) for a variety of pressure gradients and transpiration boundary conditions. It is worth noting that $l = 0{\cdot}41y$ is a common 'asymptote' for all the experimental boundary layers for small values of y/δ_{99}, where δ_{99} is defined by $u(\delta_{99}) = 0{\cdot}99u_\infty$.

Figure 7 (*b*) shows experimental values of the ratio l/y plotted against y/A, the argument in the van Driest expression for the mixing-length behaviour near a wall:

$$l = Ky[1 - \exp(-y/A)], \tag{12}$$

where K is von Kármán's constant. It may be observed that the van Driest function (with $K = 0{\cdot}41$) provides an acceptable description of the mixing-length behaviour in the wall region.

On the basis of figures 7 (*a*) and (*b*) it may be concluded that there exists a range of y close to the wall where $l = Ky$. Moreover the von Kármán constant K has

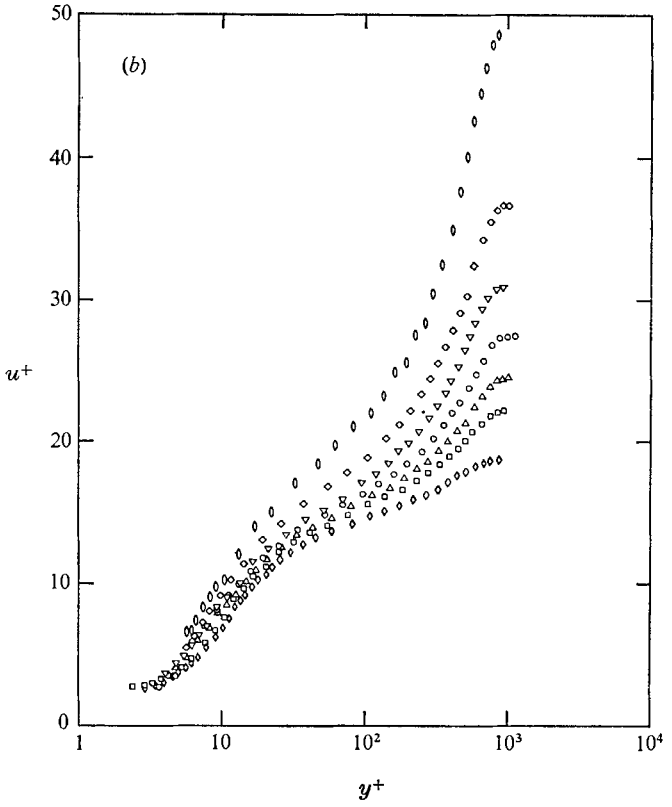

FIGURE 6. Velocity profiles in wall co-ordinates. (*a*) Constant pressure and two adverse pressure gradients without transpiration; $x = 70$ in. ——, $u^+ = (0{\cdot}41)^{-1} \ln y^+ + 5{\cdot}0$. (*b*) 'Weak' adverse pressure gradient ($m = -0{\cdot}15$); transpiration boundary condition according to (5) with $m_F = -0{\cdot}17$; $x = 82$ in.

		0	◇	▽	○	△	□	◇
(*a*)	m	—	—	−0·15	0	—	−0·20	—
	Re	—	—	3177	2574	—	3673	—
(*b*)	F_1	0·004	0·002	0·001	0	−0·001	−0·002	−0·004
	B	6·1	1·77	0·64	0	−0·39	−0·64	−0·91
	Re	6870	5097	4225	3495	2780	2226	1258

the same value (namely = 0·41) for all the experimental flows. The range in which the mixing length is proportional to the distance from the wall corresponds to the logarithmic region for the mean velocity profiles.

The experimental values of A^+ ($\equiv Au_\tau/\nu$) have been expressed as a function of p^+ ($\equiv (\nu/\rho u_\tau^3)\, dp/dx$) and v_0^+ ($\equiv v_0/u_\tau$) by the method of least squares. The best fit was obtained by the following expression:

$$A^+ = 24 \exp\left(\sum_{i=0}^{2} \sum_{j=0}^{1} a_{ij} [\ln (v_0^+ + 0{\cdot}08)]^i [\ln (p^+ + 0{\cdot}04)]^j \right), \tag{13}$$

where

$$\{a_{ij}\} = \begin{Bmatrix} -6{\cdot}71751 & -1{\cdot}50414 \\ -4{\cdot}81589 & -1{\cdot}24311 \\ -1{\cdot}27827 & -0{\cdot}388216 \end{Bmatrix}.$$

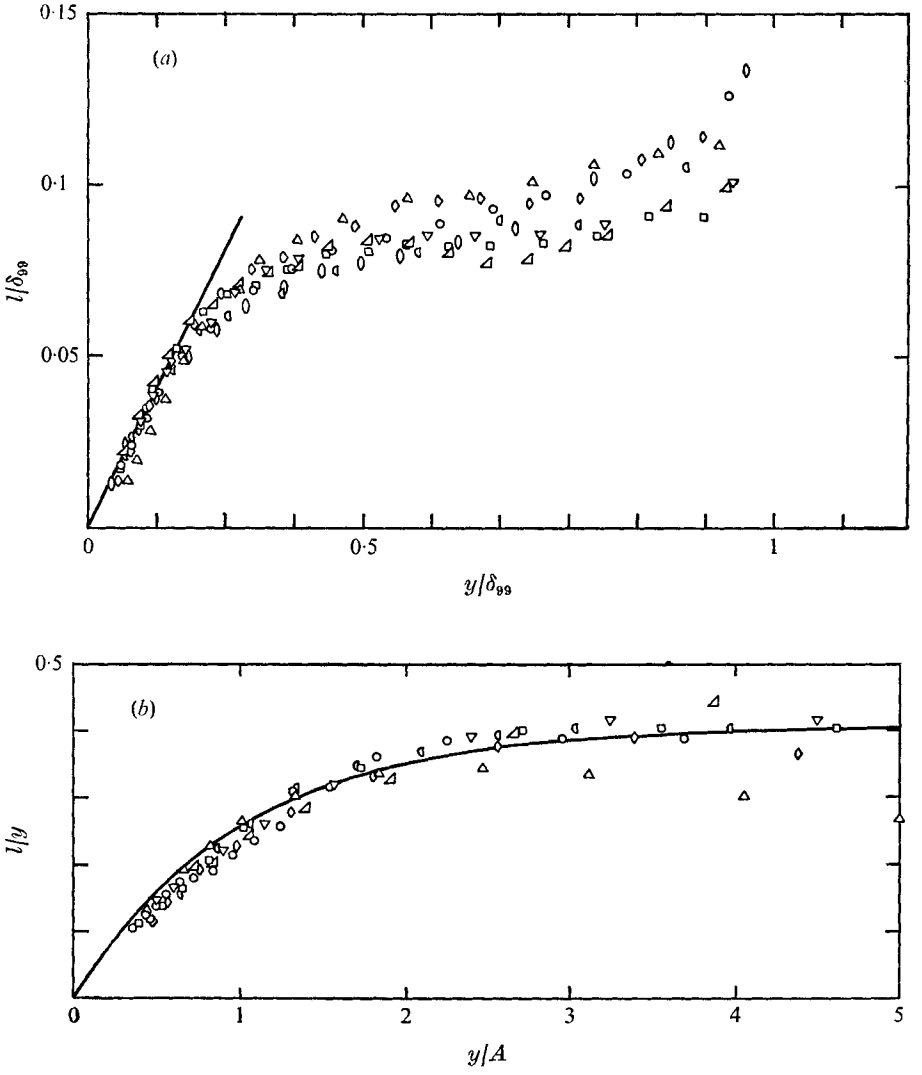

FIGURE 7. (*a*) Profiles of non-dimensional mixing length in outer region: comparison for various boundary conditions; x = 70 or 82 in. ——, $l = 0{\cdot}41y$. (*b*) Profiles of normalized mixing length *vs.* distance from the wall divided by van Driest length scale; x = 70 in. ——, $l/y = 0{\cdot}41[1-\exp(-y/H)]$.

	○	○	△	▷	▽	◁	◿	□
m	0	0	−0·15	−0·15	−0·15	−0·15	−0·15	−0·20
F_1	0	0·002	−0·004	−0·001	0	0·001	0·004	0
m_F	0	0	−0·17	0	0	0	−0·17	0

Figure 8 is a graphical display of the A^+ correlation represented by (12). It is seen that A^+ depends strongly upon the dimensionless pressure gradient $p^+ = (\nu/\rho u_\tau^3)\,dp/dx$ and the dimensionless transpiration rate $v_0^+ = v_0/u$.

A re-examination of all the results from the Stanford Heat and Mass Transfer Project, including those obtained earlier for accelerating flows ($p^+ < 0$) and

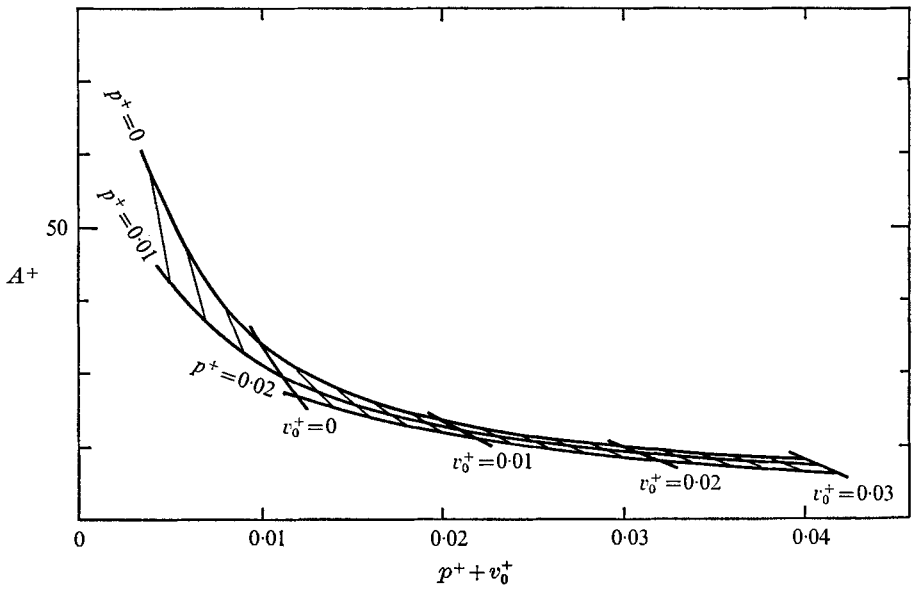

FIGURE 8. Empirical correlation for A^+ from (13).

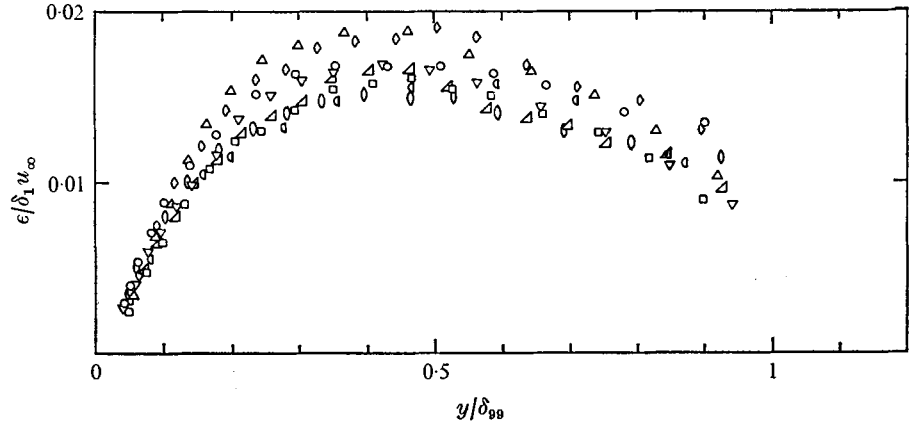

FIGURE 9. Profiles of non-dimensional eddy viscosity in outer region: comparison for selected boundary conditions; x = 70 or 82 in. Symbols as in figure 7.

Run	m	F_1	m_F
122 271–2	−0·15	−0·004	0
111 771–3	−0·15	0·002	−0·17
021 572–5	−0·20	−0·002	−0·16

TABLE 3. Runs for which a full set of data is presented.

x (in.)\Run	122 271–2	111 771–3	021 572–5
2	29·53	29·36	29·31
4	28·97	28·76	28·63
6	28·29	27·98	27·75
8	27·57	27·20	26·78
10	26·93	26·48	25·96
12	26·27	25·82	25·21
14	25·92	25·49	24·63
16	25·49	25·07	24·04
18	25·01	24·66	23·43
20	24·72	24·36	23·02
22	24·42	24·07	22·57
24	24·12	23·84	22·19
26	23·92	23·61	21·87
28	23·69	23·39	21·53
30	23·43	23·15	21·23
32	23·23	22·97	20·97
34	23·04	22·76	20·68
36	22·83	22·60	20·48
38	22·65	22·42	20·24
40	22·54	22·26	20·09
42	22·32	22·10	19·88
44	22·19	21·96	19·73
46	22·05	21·82	19·55
48	21·91	21·66	19·42
50	21·80	21·52	19·27
52	21·66	21·41	19·17
54	21·58	21·30	19·95
56	21·46	21·16	18·95
58	21·41	21·07	18·79
60	21·26	20·98	18·70
62	21·21	20·87	18·60
64	21·09	20·78	18·54
66	21·01	20·70	18·44
68	20·89	20·61	18·34
70	20·83	20·55	18·24
72	20·77	20·47	18·14
74	20·69	20·41	18·08
76	20·60	20·32	17·94
78	20·54	20·26	17·88
80	20·42	20·17	17·77
82	20·39	20·08	17·67
84	20·27	20·02	17·57
86	20·18	19·96	17·43
88	20·18	19·87	17·36
90	20·03	19·81	17·23
92	20·00	19·75	17·12

TABLE 4. Measured free-stream velocity distributions u_∞ (ft/s)

including the newer data for transpiration with no pressure gradient and with an adverse pressure gradient ($p^+ > 0$), leads to the following empirical equation:

$$A^+ = \frac{24{\cdot}0}{a[v_0^+ + bp^+/(1+cv_0^+)] + 1{\cdot}0},$$

x (in.)\Run	122 271–2	111 771–3	021 572–5
2	−0·00399	0·00200	−0·00201
6	−0·00399	0·00192	−0·00190
10	−0·00398	0·00181	−0·00177
14	−0·00397	0·00173	−0·00167
18	−0·00400	0·00168	−0·00164
22	−0·00399	0·00161	−0·00159
26	−0·00399	0·00157	−0·00154
30	−0·00400	0·00155	−0·00152
34	−0·00400	0·00152	−0·00151
38	−0·00399	0·00149	−0·00146
42	−0·00400	0·00148	−0·00144
46	−0·00401	0·00145	−0·00143
50	−0·00401	0·00144	−0·00142
54	−0·00399	0·00138	−0·00139
58	−0·00399	0·00139	−0·00138
62	−0·00398	0·00138	−0·00136
66	−0·00400	0·00136	−0·00133
70	−0·00399	0·00135	−0·00132
74	−0·00398	0·00133	−0·00131
78	−0·00398	0·00132	−0·00130
82	−0·00399	0·00131	−0·00130
86	−0·00399	0·00131	−0·00130
90	−0·00401	0·00129	−0·00129
92	−0·00399	0·00128	−0·00128

TABLE 5. Measured blowing fractions F

where $a = 9{\cdot}0$ if $v_0^+ < 0$, otherwise $a = 7{\cdot}1$. If $p^+ > 0$ then $b = 2{\cdot}9$ and $c = 0$, otherwise $b = 4{\cdot}25$ and $c = 10{\cdot}0$.

Note that the van Driest length scale as defined here is normalized with respect to the wall shear stress, and not the local shear stress as has sometimes been done.

The eddy diffusivity ϵ is defined by

$$-\overline{u'v'} = \epsilon\, du/dy. \tag{14}$$

The non-dimensional eddy diffusivity $k = \epsilon/\delta_1 u_\infty$ is plotted versus y/δ_{99} in figure 9. It may be observed that neither the pressure gradient nor transpiration rate has much effect in the outer region.

A full set of mean velocity and turbulence intensity data is presented for the three runs in table 3. The measured free-stream velocity distributions are given in table 4; the measured blowing fractions are listed in table 5. A complete list of all the experimental data related to the mean velocity profiles is presented in table 6. The friction coefficients given in this table are taken from smooth fits of the experimental values presented in figure 3.

The profiles of the intensities of the three components of the turbulent fluctuations are presented in figures 10 (*a*)–(*c*). The corresponding profiles of the Reynolds stress are presented in figures 11(*a*)–(*c*)

Note. The free-stream velocities listed in the profile table 6 are hot-wire results

Run 122 271–2: $m = -0{\cdot}15$, $m_F = 0$ ($\nu = 1{\cdot}61 \times 10^{-4}$)

x	u_∞	F	Re	$\frac{1}{2}c_f$	β	B	G
2	29·32	−0·00399	451	0·00397	0·073	−1·006	4·84
10	26·81	−0·00398	557	0·00380	0·174	−1·046	4·75
22	24·29	−0·00399	662	0·00383	0·111	−1·041	4·43
34	22·95	−0·00400	712	0·00381	0·084	−1·050	4·13
46	22·07	−0·00401	761	0·00379	0·070	−1·059	4·04
58	21·45	−0·00399	773	0·00377	0·059	−1·059	3·99
70	20·77	−0·00399	788	0·00376	0·051	−1·061	3·74
82	20·38	−0·00399	814	0·00375	0·046	−1·065	3·81
90	20·14	−0·00401	822	0·00375	0·045	−1·068	3·63

$x = 2$		$x = 10$		$x = 22$		$x = 34$		$x = 46$		$x = 58$		$x = 70$		$x = 82$		$x = 90$	
y	u	y	u	y	u	y	u	y	u	y	u	y	u	y	u	y	u
0·004	5·81	0·005	6·66	0·005	4·74	0·006	5·15	0·005	4·01	0·005	3·72	0·005	4·14	0·005	3·79	0·007	4·95
0·005	6·52	0·006	7·53	0·006	4·94	0·007	5·76	0·006	4·57	0·006	3·96	0·006	4·19	0·006	4·15	0·008	5·42
0·006	7·41	0·007	8·54	0·007	5·57	0·008	6·31	0·007	5·27	0·007	4·37	0·007	4·75	0·007	4·69	0·009	6·07
0·007	8·25	0·008	9·48	0·008	6·28	0·009	6·88	0·008	6·04	0·008	5·04	0·008	5·45	0·008	5·11	0·010	6·58
0·008	9·21	0·009	10·20	0·009	6·96	0·010	7·64	0·009	6·62	0·009	5·56	0·009	6·48	0·009	5·83	0·011	7·20
0·010	11·25	0·011	11·59	0·011	8·32	0·012	8·98	0·011	8·06	0·011	7·10	0·011	7·89	0·011	6·88	0·012	8·17
0·012	12·75	0·013	12·75	0·013	9·96	0·014	10·14	0·013	9·18	0·013	8·24	0·013	9·10	0·013	8·09	0·014	9·07
0·014	14·37	0·015	13·74	0·015	11·21	0·016	11·29	0·015	10·34	0·015	9·45	0·015	10·26	0·015	9·22	0·016	9·99
0·016	15·47	0·017	14·56	0·017	12·38	0·019	12·81	0·018	11·71	0·017	10·67	0·017	11·05	0·017	10·15	0·018	11·03
0·018	16·51	0·020	15·64	0·019	13·22	0·022	13·80	0·021	12·84	0·019	11·85	0·019	11·73	0·020	11·42	0·020	11·59
0·020	17·11	0·023	16·37	0·022	14·48	0·025	14·79	0·024	13·79	0·021	12·56	0·022	12·66	0·023	12·49	0·023	12·47
0·023	18·15	0·027	17·33	0·025	15·38	0·029	15·62	0·028	14·64	0·023	13·19	0·025	13·45	0·026	13·41	0·026	13·19
0·026	18·91	0·033	18·55	0·028	16·14	0·033	16·32	0·033	15·75	0·026	14·21	0·029	14·17	0·030	14·17	0·030	14·12
0·029	19·55	0·041	19·52	0·032	16·74	0·038	17·08	0·039	16·58	0·029	14·77	0·033	15·04	0·036	15·30	0·034	14·82
0·033	20·27	0·051	20·32	0·037	17·52	0·046	18·06	0·047	17·35	0·033	15·36	0·038	15·86	0·041	15·92	0·038	15·58
0·038	21·15	0·063	21·26	0·043	18·30	0·056	18·87	0·059	18·23	0·037	16·07	0·043	16·43	0·046	16·53	0·043	16·06
0·044	21·79	0·078	21·98	0·051	18·98	0·071	19·60	0·074	19·08	0·042	16·76	0·053	17·06	0·056	17·28	0·053	16·74
0·052	22·57	0·093	22·71	0·061	19·75	0·091	20·45	0·094	19·88	0·047	17·22	0·063	17·77	0·071	18·10	0·068	17·90
0·062	23·31	0·113	23·42	0·076	20·46	0·121	21·35	0·119	20·56	0·056	17·80	0·078	18·52	0·096	18·99	0·083	18·36
0·072	23·98	0·133	24·18	0·096	21·32	0·161	22·40	0·149	21·30	0·066	18·50	0·103	19·14	0·121	19·65	0·108	19·07
0·087	24·85	0·158	25·08	0·116	22·02	0·201	23·28	0·199	22·44	0·081	19·17	0·128	19·90	0·146	20·21	0·133	19·96
0·102	25·60	0·198	26·30	0·141	22·75	0·241	24·01	0·249	23·32	0·106	19·98	0·178	20·97	0·196	20·96	0·158	20·23
0·117	26·27	0·238	27·43	0·171	23·52	0·291	24·90	0·299	24·14	0·131	20·61	0·228	21·84	0·246	21·96	0·208	21·07
0·137	27·12	0·278	28·44	0·206	24·40	0·341	25·75	0·349	24·85	0·181	21·66	0·303	22·93	0·321	22·72	0·258	21·76
0·157	27·91	0·318	29·33	0·256	25·48	0·391	26·54	0·399	25·53	0·231	22·49	0·378	23·92	0·396	23·64	0·333	22·77
0·182	28·72	0·373	30·24	0·306	26·50	0·441	27·24	0·474	26·51	0·281	23·30	0·453	24·66	0·496	24·57	0·408	23·56
0·207	29·45	0·423	30·83	0·356	27·52	0·491	27·98	0·549	27·41	0·331	23·99	0·553	25·78	0·596	25·58	0·508	24·55
0·247	30·32	0·473	31·06	0·406	28·36	0·566	28·89	0·624	28·22	0·406	24·95	0·653	26·74	0·696	26·46	0·608	25·52
0·287	30·90	0·523	31·14	0·456	29·15	0·641	29·69	0·699	28·94	0·481	25·83	0·753	27·59	0·846	27·60	0·708	26·19
0·332	31·16	0·598	31·15	0·531	30·12	0·716	30·14	0·799	29·81	0·581	26·91	0·853	28·37	0·996	28·63	0·858	27·30
0·382	31·22	0·673	31·13	0·606	30·75	0·791	30·78	0·899	30·51	0·681	27·94	1·003	29·49	1·146	29·56	1·008	28·36
0·432	31·21			0·681	31·05	0·891	31·00	0·999	30·88	0·806	28·98	1·153	30·29	1·346	30·44	1·208	29·50
				0·756	31·14	0·991	31·05	1·099	31·03	0·956	30·13	1·303	30·83	1·546	30·91	1·408	30·38
				0·856	31·14	1·091	31·05	1·199	31·06	1·106	30·82	1·503	31·05	1·796	31·06	1·708	31·02
								1·424	31·04	1·506	31·15	1·878	31·04			2·308	31·04
										1·706	31·13					2·608	31·05
																2·808	31·06
																3·108	31·06

TABLE 6. Profile data. Lengths in in., velocities in ft/s, kinematic viscosity in ft²/s

Run 111 771–3: $m = -0{\cdot}15$, $m_P = -0{\cdot}17$ ($\nu = 1{\cdot}60 \times 10^{-4}$)

x	u_∞	F	Re	$\frac{1}{2}c_f$	β	B	G
2	29·26	0·00200	587	0·00230	0·187	0·871	8·00
10	26·59	0·00181	1219	0·00150	1·165	1·207	10·56
22	24·11	0·00161	2062	0·00108	1·542	1·491	12·64
34	22·78	0·00152	2758	0·00087	1·806	1·751	13·88
46	21·79	0·00145	3412	0·00082	1·853	1·768	14·30
58	20·96	0·00139	3973	0·00079	1·820	1·757	14·17
70	20·46	0·00135	4544	0·00076	1·839	1·769	14·16
82	20·00	0·00131	5097	0·00074	1·897	1·765	14·25
90	19·73	0·00129	5471	0·00073	2·053	1·771	14·28

$x = 2$		$x = 10$		$x = 22$		$x = 34$		$x = 46$		$x = 58$		$x = 70$		$x = 82$		$x = 90$	
y	u	y	u	y	u	y	u	y	u	y	u	y	u	y	u	y	u
0·004	4·19	0·005	3·01	0·010	3·02	0·012	2·99	0·014	2·55	0·017	2·89	0·020	3·47	0·020	2·98	0·020	3·24
0·005	4·58	0·007	3·63	0·012	3·47	0·014	3·43	0·016	2·96	0·019	3·29	0·022	3·66	0·023	3·42	0·023	3·66
0·006	5·28	0·009	4·34	0·014	3·93	0·016	3·93	0·018	3·22	0·021	3·57	0·024	3·97	0·026	3·95	0·026	4·06
0·008	6·74	0·011	5·20	0·016	4·50	0·018	4·34	0·020	3·73	0·023	3·94	0·026	4·26	0·029	4·40	0·029	4·28
0·010	8·20	0·013	5·97	0·019	5·23	0·020	4·88	0·022	3·95	0·026	4·34	0·029	4·64	0·034	4·97	0·039	4·83
0·012	9·50	0·016	7·16	0·022	5·96	0·023	5·27	0·025	4·57	0·031	5·17	0·034	5·39	0·041	5·56	0·046	5·40
0·014	10·81	0·019	8·13	0·026	6·65	0·027	5·87	0·030	5·44	0·038	5·86	0·042	5·95	0·051	6·22	0·056	6·15
0·016	11·75	0·022	9·00	0·032	7·81	0·033	6·53	0·037	6·18	0·048	6·84	0·054	6·79	0·068	7·17	0·063	6·65
0·018	12·72	0·026	9·78	0·041	8·72	0·041	7·50	0·047	6·98	0·060	7·45	0·072	7·49	0·093	7·79	0·078	7·16
0·020	13·53	0·030	10·40	0·051	9·47	0·053	8·34	0·062	7·77	0·075	7·94	0·097	8·13	0·133	8·51	0·103	7·61
0·022	14·15	0·035	11·05	0·063	10·04	0·070	9·08	0·087	8·75	0·100	8·63	0·137	8·99	0·198	9·17	0·143	8·50
0·025	14·96	0·041	11·68	0·078	10·61	0·095	9·95	0·122	9·28	0·140	9·22	0·197	9·57	0·273	9·58	0·213	9·09
0·028	15·74	0·048	12·34	0·098	11·26	0·130	10·73	0·162	10·09	0·195	9·93	0·257	10·04	0·373	10·31	0·313	9·70
0·032	16·60	0·056	12·77	0·128	12·06	0·170	11·34	0·217	10·68	0·260	10·61	0·357	10·53	0·498	11·04	0·413	10·12
0·036	17·20	0·071	13·70	0·163	12·70	0·220	11·85	0·277	11·19	0·335	11·14	0·457	11·36	0·623	11·56	0·538	11·05
0·040	17·79	0·091	14·55	0·198	13·37	0·270	12·50	0·352	12·07	0·410	11·68	0·557	11·66	0·748	12·17	0·663	11·43
0·045	18·32	0·116	15·47	0·238	14·01	0·345	13·24	0·427	12·60	0·510	12·19	0·657	12·38	0·898	12·75	0·738	11·57
0·050	18·87	0·146	16·55	0·283	14·60	0·420	14·11	0·502	13·18	0·610	12·66	0·782	13·16	1·048	13·29	0·813	11·88
0·057	19·54	0·181	17·50	0·333	15·44	0·495	14·82	0·602	13·92	0·710	13·42	0·907	13·65	1·198	13·93	0·963	12·60
0·065	20·18	0·216	18·61	0·383	16·19	0·570	15·63	0·702	14·60	0·835	14·11	1·032	14·14	1·348	14·55	1·113	13·16
0·075	20·98	0·251	19·61	0·433	16·97	0·645	16·34	0·802	15·28	0·960	14·79	1·157	14·74	1·498	15·20	1·263	13·74
0·088	21·76	0·286	20·57	0·483	17·74	0·720	17·13	0·927	16·82	1·085	15·63	1·307	15·46	1·698	15·85	1·413	14·25
0·103	22·72	0·321	21·55	0·533	18·40	0·795	17·73	1·052	17·33	1·210	16·32	1·457	16·20	1·898	16·51	1·613	14·83
0·118	23·45	0·356	22·41	0·583	19·15	0·895	18·76	1·177	18·04	1·360	17·09	1·607	16·76	2·198	17·67	1·813	15·56
0·133	24·21	0·391	23·30	0·633	19·83	0·995	19·71	1·302	18·97	1·510	17·93	1·757	17·41	2·498	18·66	2·013	16·15
0·153	25·04	0·431	24·20	0·683	20·54	1·095	20·53	1·452	19·84	1·660	18·66	1·907	17·98	2·798	19·36	2·313	17·11
0·178	26·04	0·471	24·98	0·733	21·22	1·195	21·34	1·602	20·63	1·810	19·33	2·107	18·79	3·098	19·81	2·613	18·05
0·208	26·99	0·521	25·76	0·783	21·82	1·295	21·95	1·752	21·28	2·010	20·13	2·307	19·40	3·398	19·95	2·913	18·86
0·238	27·75	0·571	26·28	0·833	22·38	1·395	22·38	1·902	21·63	2·210	20·63	2·507	19·97	3·698	20·01	3·213	19·36
0·268	28·37	0·621	26·52	0·908	23·18	1·520	22·68	2·102	21·81	2·410	20·89	2·807	20·40	3·898	20·00	3·513	19·66
0·308	28·90	0·696	26·59	1·008	23·81	1·645	22·78	2·302	21·82	2·710	20·98	3·207	20·49			3·913	19·76
0·358	29·21	0·796	26·59	1·108	24·07	1·770	22·78	2·502	21·79	3·010	20·96	3·607	20·46			4·413	19·73
0·408	29·27			1·208	24·11	1·885	22·78										
0·468	29·27			1·333	24·11												
0·528	29·26																

TABLE 6 (*continued*)

Run 021 572–5: $m = -0{\cdot}20$, $m_F = -0{\cdot}16$ ($\nu = 1{\cdot}60 \times 10^{-4}$)

x	u_∞	F	Re	$\frac{1}{2}c_f$	β	B	G
2	29·42	−0·00201	519	0·00276	0·194	−0·728	6·37
10	26·05	−0·00177	801	0·00246	0·611	−0·720	6·72
22	22·55	−0·00159	1250	0·00221	0·590	−0·719	7·20
34	20·69	−0·00151	1608	0·00208	0·571	−0·726	7·12
46	19·49	−0·00143	1911	0·00198	0·565	−0·722	7·25
58	18·73	−0·00138	2121	0·00193	0·524	−0·715	7·01
70	18·10	−0·00132	2381	0·00186	0·518	−0·710	6·96
82	17·53	−0·00130	2619	0·00182	0·505	−0·714	7·00
90	17·02	−0·00129	2860	0·00179	0·542	−0·721	7·20

$x = 2$		$x = 10$		$x = 22$		$x = 34$		$x = 46$		$x = 58$		$x = 70$		$x = 82$		$x = 90$	
y	u	y	u	y	u	y	u	y	u	y	u	y	u	y	u	y	u
0·004	5·81	0·005	4·60	0·005	3·00	0·006	3·08	0·007	2·52	0·008	2·78	0·006	2·58	0·008	2·61	0·010	2·70
0·005	6·63	0·006	5·10	0·006	3·18	0·007	3·38	0·008	2·81	0·009	3·00	0·007	2·85	0·009	2·79	0·011	2·92
0·006	7·22	0·007	6·13	0·007	3·61	0·008	3·75	0·009	3·07	0·011	3·47	0·008	2·96	0·011	3·19	0·013	3·32
0·007	8·40	0·008	6·76	0·008	3·80	0·009	4·08	0·011	3·68	0·013	4·06	0·009	3·21	0·013	3·70	0·015	3·69
0·008	9·09	0·009	7·28	0·009	4·23	0·010	4·48	0·013	4·23	0·015	4·52	0·011	3·75	0·016	4·23	0·018	4·35
0·010	10·94	0·010	7·67	0·011	4·87	0·011	4·76	0·015	4·90	0·018	5·32	0·013	4·21	0·019	4·97	0·023	5·13
0·012	12·59	0·012	8·87	0·013	5·81	0·013	5·53	0·018	5·62	0·021	6·09	0·016	4·86	0·024	5·89	0·028	5·97
0·014	13·87	0·014	9·94	0·015	6·49	0·015	6·13	0·021	6·38	0·024	6·73	0·019	5·45	0·029	6·68	0·038	7·17
0·016	15·15	0·016	10·78	0·018	7·65	0·018	6·93	0·024	7·00	0·028	7·38	0·023	6·32	0·039	7·73	0·048	7·64
0·018	16·09	0·018	11·71	0·021	8·61	0·021	7·72	0·028	7·62	0·033	8·03	0·028	7·01	0·049	8·50	0·063	8·40
0·021	17·08	0·021	12·05	0·024	9·35	0·025	8·36	0·033	8·37	0·038	8·52	0·033	7·72	0·064	9·18	0·083	9·06
0·024	17·93	0·024	13·29	0·028	10·13	0·030	9·22	0·038	8·95	0·048	9·28	0·043	8·57	0·079	9·65	0·133	9·65
0·027	18·67	0·027	14·00	0·032	10·68	0·035	9·84	0·048	9·69	0·058	9·93	0·053	9·19	0·099	10·10	0·163	10·17
0·031	19·31	0·031	14·58	0·039	11·62	0·043	10·39	0·063	10·43	0·073	10·38	0·068	9·74	0·149	10·63	0·213	10·46
0·035	19·91	0·036	15·25	0·049	12·32	0·053	11·11	0·078	10·98	0·088	10·89	0·083	10·23	0·199	11·02	0·313	11·08
0·043	20·69	0·042	15·97	0·059	12·98	0·068	11·73	0·098	11·39	0·108	11·28	0·103	10·53	0·299	11·77	0·463	11·56
0·048	21·25	0·049	16·39	0·079	13·70	0·093	12·28	0·148	12·11	0·158	11·80	0·153	11·20	0·399	12·00	0·613	12·20
0·058	21·92	0·059	16·96	0·109	14·35	0·143	13·10	0·198	12·62	0·208	12·27	0·203	11·60	0·549	12·68	0·813	12·93
0·068	22·45	0·079	17·92	0·159	15·29	0·193	13·72	0·273	13·17	0·308	12·93	0·303	12·20	0·699	13·28	1·013	13·61
0·078	23·00	0·099	18·65	0·209	16·01	0·268	14·46	0·348	13·75	0·408	13·45	0·403	12·79	0·899	13·99	1·313	14·50
0·098	23·93	0·139	19·76	0·284	17·19	0·343	15·17	0·448	14·33	0·558	14·22	0·553	13·39	1·099	14·72	1·613	15·24
0·118	24·71	0·179	20·79	0·359	18·13	0·443	16·13	0·548	15·15	0·708	15·00	0·703	14·05	1·399	15·63	1·813	15·89
0·148	25·84	0·219	21·74	0·434	19·15	0·543	17·00	0·698	16·11	0·908	16·00	0·903	14·92	1·699	16·52	2·113	16·50
0·178	26·77	0·259	22·63	0·509	20·10	0·643	17·87	0·848	17·04	1·108	16·95	1·103	15·66	1·999	17·16	2·413	16·88
0·208	27·61	0·299	23·50	0·609	21·13	0·743	18·69	0·998	17·91	1·308	17·75	1·403	16·76	2·299	17·47	2·713	17·01
0·258	28·64	0·349	24·38	0·709	22·00	0·893	19·71	1·198	18·83	1·508	18·36	1·703	17·61	2·499	17·55	3·013	17·02
0·308	29·14	0·399	25·16	0·809	22·41	1·043	20·37	1·398	19·37	1·708	18·67	2·003	18·05	2·599	17·53		
0·383	29·38	0·474	25·83	0·909	22·55	1·193	20·65	1·598	19·50	1·858	18·73	2·303	18·09				
0·458	29·40	0·549	26·05	1·009	22·55	1·393	20·69	1·748	19·49	1·883	18·73	2·403	18·10				
0·508	29·42	0·624	26·07														
		0·699	26·05														

TABLE 6 (*continued*)

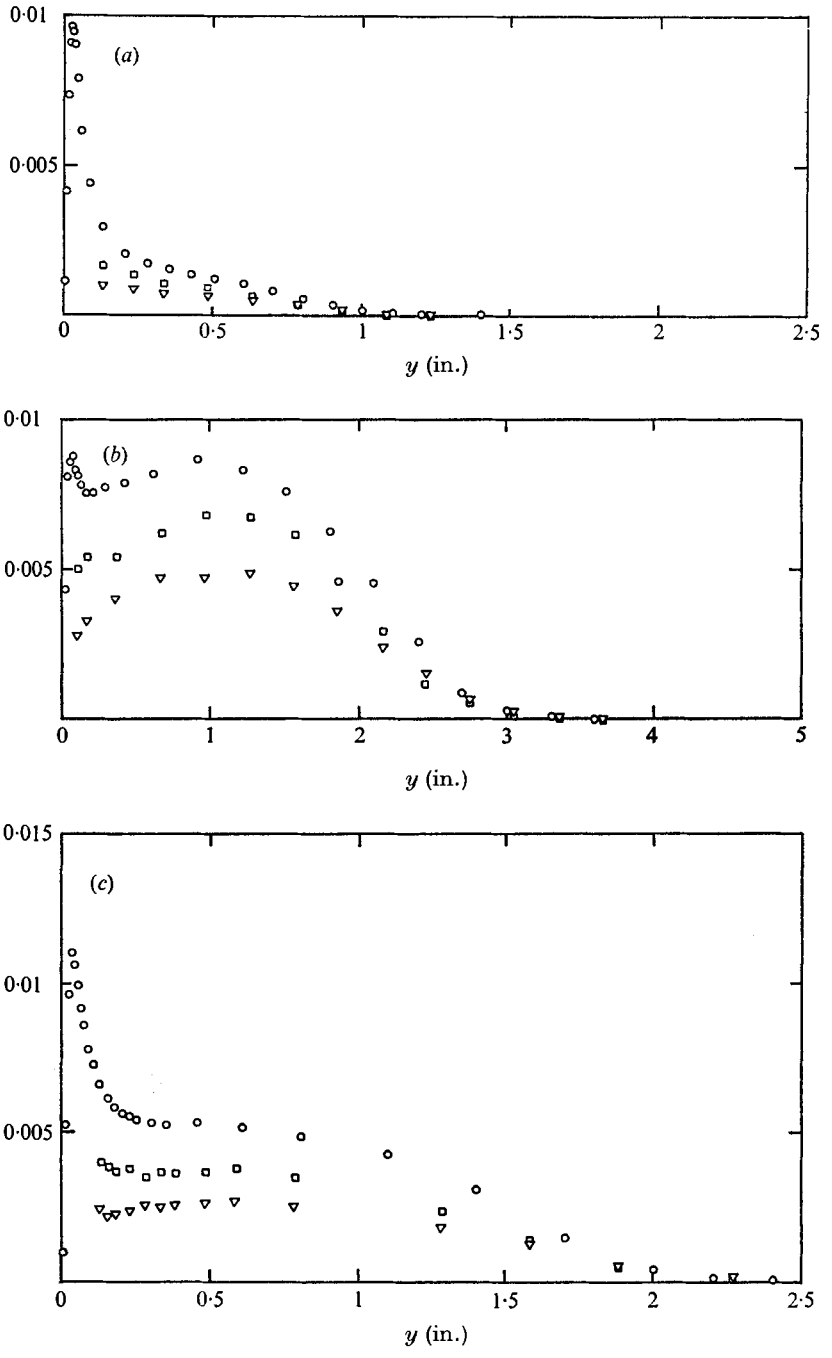

FIGURE 10. Profiles of the three turbulence intensities. (*a*) 'Weak' adverse pressure gradient ($m = -0{\cdot}15$) with suction ($F = -0{\cdot}004$); $x = 70$ in.; $Re = 788$ (run 122 271–2). (*b*) 'Weak' adverse pressure gradient ($m = -0{\cdot}15$) with blowing ($F = 0{\cdot}00135$); $x = 70$ in.; $Re = 4544$ (run 111 771–3). (*c*) 'Strong' adverse pressure gradient ($m = -0{\cdot}20$) with suction ($F = -0{\cdot}00132$); $x = 70$ in.; $Re = 2381$ (run 021 572–5). ○, $\overline{u'^2}/u_\infty^2$; ▽, $\overline{v'^2}/u_\infty^2$; □, $\overline{w'^2}/u_\infty^2$.

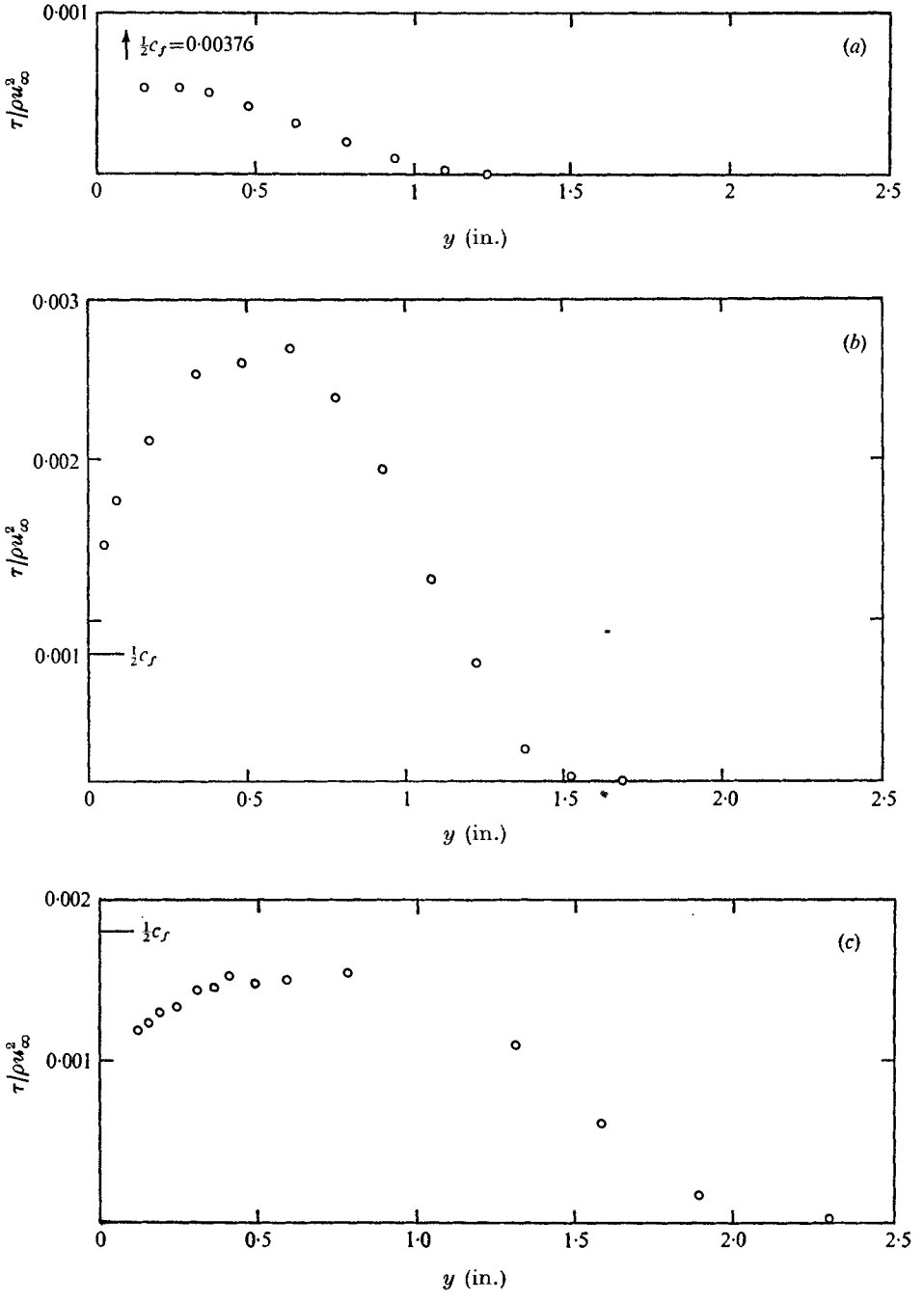

FIGURE 11. Measured profiles of the Reynolds stress $-\overline{u'v'}/u_\infty^2$ for the same three runs as in figure 10.

corresponding to the last profile points, whereas the free-stream velocity distributions listed in table 4 were computed from the pressure distribution. As a consequence slight discrepancies between the two quotations of u_∞ may be found. The pressure gradient is computed on the basis of the velocities in table 4.

6. Summary and conclusions

Experimental results for turbulent incompressible boundary layers with transpiration are presented both for constant-pressure and adverse-pressure-gradient conditions. The three different free-stream velocity distributions may be described by equations of the form

$$u_\infty \propto u_1 x^m, \quad \text{where} \quad m = 0, \; -0{\cdot}15, \; -0{\cdot}20. \tag{15}$$

The transpiration boundary conditions may be expressed by

$$F \propto F_1 m^{m_F}, \quad \text{where} \quad -0{\cdot}004 \leqslant F_1 \leqslant -0{\cdot}008, \; -0{\cdot}17 \leqslant m_F \leqslant 0. \tag{16}$$

In addition to mean velocity profiles and Reynolds-stress profiles, profiles of the three turbulence intensities were measured. The skin friction was determined by a technique involving the measurement of the shear stress close to the wall (as the sum of the Reynolds stress and the viscous stress) and then 'extrapolating' to the wall using the integrated boundary-layer equations.

The following conclusions are presented.

(i) Although the friction coefficient depends strongly upon the pressure gradient, the ratio $(c_f/c_{f0})_{m,\,Re}$ is a function of only the blowing parameter $B \equiv 2F/c_f$ (or equivalently of $B_0 \equiv 2F/c_{f0}$) for the range of pressure gradients and Reynolds numbers covered by the experiments.

(ii) Clauser-type equilibrium boundary layers (i.e. flows having a constant Clauser shape factor G) are obtained for constant values of the Clauser pressure-gradient parameter β and the blowing parameter B. Furthermore it is shown that G is a function of $\beta + B$, and that β and B have identical effects upon the shape of the defect profile.

(iii) For all the experimental boundary layers there exists a range of y, the 'logarithmic region', where the mixing length may be expressed as

$$l = Ky \quad (K = 0{\cdot}41). \tag{17}$$

The von Kármán constant K is therefore independent of both the transpiration rate and pressure gradient for near-equilibrium boundary layers.

(iv) Values of the van Driest length scale A^+ were computed and are presented in the form $A^+(p^+, v_0^+)$.

This work was supported in part by the National Aeronautics and Space Administration Grant NGL 05-020-134. The interest and help of Dr R. W. Graham are particularly appreciated.

REFERENCES

ANDERSEN, P. S., KAYS, W. M. & MOFFAT, R. J. 1972 *Thermosci. Div., Stanford University Rep.* HMT-15.

BRADSHAW, P. 1967 *J. Fluid Mech.* **29**, 625.

CLAUSER, F. H. 1954 *J. Aero. Sci.* **21**, 91.

COLES, D. E. 1962 *Rand Corp. Rep.* R-403-PR.

JULIEN, H. L., KAYS, W. M. & MOFFAT, R. J. 1971 *A.S.M.E. J. Heat Transfer*, **93**, 373–379.

KAYS, W. M. 1972 *Int. J. Heat Mass Transfer*, **15**, 1023–1044.

LOYD, R. J., MOFFAT, R. J. & KAYS, W. M. 1970 *Thermosci. Div., Stanford University Rep.* HMT-13.

MCLEAN, J. D. & MELLOR, G. L. 1972 *Int. J. Heat Mass Transfer*, **15**, 2353–2369.

MOFFAT, R. J. & KAYS, W. M. 1968 *Int. J. Heat Mass Transfer*, **11**, 1547–1566.

SIMPSON, R. N., MOFFAT, R. J. & KAYS, W. M. 1969 *Int. J. Heat Mass Transfer*, **12**, 771–789.

STEVENSON, T. N. 1963 *College of Aeronautics, Cranfield Aero. Rep.* no. 166.

YOUNG, A. D. & MAAS, J. N. 1936 *Aero. Res. Counc. R. & M.* no. 1770.